Computation of strong-field multiphoton processes in polyelectronic atoms: State-specific method and applications to H and Li⁻

Th. Mercouris, Y. Komninos, S. Dionissopoulou, and C. A. Nicolaides

Theoretical and Physical Chemistry Institute, National Hellenic Research Foundation, 48 Vassileos Constantinou Avenue, 116 35 Athens, Greece

(Received 21 April 1994)

The problem of integrating the time-dependent Schrödinger equation (TDSE) describing the interaction of a polyelectronic atom with a laser pulse is treated by expanding the time-dependent wave function $\Psi(\mathbf{r},t)$ in terms of wave functions $\Phi_{n,E}$ computed for discrete, autoionizing, and scattering states separately. The TDSE is transformed into a system of coupled first-order differential equations with time-dependent coefficients, whose number (in the thousands), necessary for convergence to be reliable, depends mainly on the degree of the contribution of the continuous spectrum, as a function of the frequency and strength of the field. This approach allows the systematic incorporation of the significant electronic structure, electron correlation, and spectral characteristics of each N-electron system under investigation. Furthermore, since the free-electron function is computed numerically in the polarized core potential of the remaining $(N-1)$-electron atom, properties such as the angular distribution and partial above-threshold ionization (ATI) of the photoelectron are directly computable. We present results from the application of our methods to H and Li⁻. For the applications to H, which served as testing grounds for the method, the state-specific wave functions for discrete and continuum states were obtained numerically, for n and l up to 12 and 5, respectively, and for positive energies up to $\varepsilon=34$ eV with l up to 6. When comparisons with other time-independent and time-dependent results are possible, very good agreement is observed. On the other hand, our calculations do not confirm recent experimental results on absolute ionization rates for laser pulses of 248 nm. For Li⁻, our results on ATI for photon energy $\hbar\omega=1.36$ eV demonstrate the effects of initial-state electron correlation and of final-state field-induced coupling of open channels (the Li $1s^2 2s\,{}^2S$ and $1s^2 2p\,{}^2P^o$), as a function of field intensity.

PACS number(s): 42.50.Hz, 32.80.Rm

I. INTRODUCTION

In recent years [1–11], it has become possible to integrate the time-dependent Schrödinger equation (TDSE) for the hydrogen atom interacting with a strong laser pulse. As a result, reliable information on aspects of the physics of this interaction became available for the first time. However, as with the time-independent Schrödinger equation, the H atom is a special case. Thus it is important and timely to develop approaches which are general and practical enough to be applicable to the challenging problem of computing the TDSE for the response of a ground or an excited state of a *polyelectronic* atom to intense and short laser pulses.

Reviews of the progress that had been made until recently regarding the solution of the TDSE for multiphoton atomic processes were published by Kulander, Schafer, and Krause [12] and by Lambropoulos and Tang [13]. Kulander, Schafer, and Krause [12] have produced a number of results and conclusions on single determinantal states where only one electron is active, either in a pure Coulomb field (hydrogen atom) or in a mean field (Hartree-Fock-Slater). On the other hand, Lambropoulos and Tang [13] have stressed the need for considering the details of atomic structure and have implemented a specialized discrete basis set method using splines for the computation of the multiphoton ionization of the ^1S state of two-electron atoms. The conclusion that one can

draw from these articles and from their quoted work is that the one-electron atom can, by now, be handled accurately (in principle at least up to intensities of 1×10^{14} W/cm² and $\lambda=1064$ nm [11]), but that it remains as a desideratum to have an approach which is applicable to many-electron atomic states, allowing the incorporation of the effects of electronic structure, of electron correlation, of single as well as of multiple excitations, and of the term-dependent continuum. The present work shows how this can be achieved and how some of the aforementioned effects can influence observable phenomena such as above-threshold ionization (ATI).

In the following sections, we present our approach and a few applications to two atoms, H and Li⁻. For hydrogen we used the exact discrete and scattering functions, computed numerically. This served to check the correctness of our numerical methods, in particular the accuracy of the continuum-continuum dipole matrix elements (computed using numerical functions), and of the overall technique of integrating the TDSE. In addition, H offered the opportunity of making comparisons with previous theoretical and experimental results. Applications to the phenomena of harmonic generation (HG) and of angular distributions are reported elsewhere [14].

On the other hand, Li⁻ ^1S was chosen as a manageable and interesting negative ion system where the singlet discrete spectrum is missing. This implies that the result of the major interelectronic interactions in the initial

Li⁻
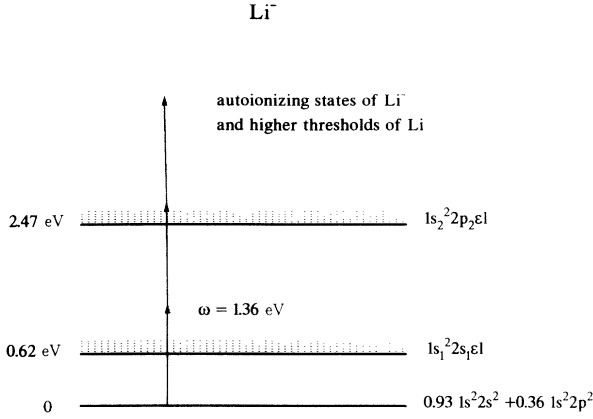
FIG. 1. The part of the spectrum of Li⁻ and of Li studied in this work.

state ought to be easily reflected on the photoelectron spectrum. The major components of the Li⁻ ^1S ground state are the $1s^22s^2$ and $1s^22p^2$ configurations, whose coefficients from a multiconfigurational Hartree-Fock (MCHF) calculation are 0.933 and 0.360, respectively. In Sec. IV we show the effect of this initial-state configurational mixing on the photoelectron spectra, which is revealed as a function of the field intensity. Another prototypical feature of the Li⁻ system is that with only small excitation energies, more than one channel opens up in the final state (Fig. 1). Specifically, the first ionization threshold, the Li $1s^22s$ ^2S state, is 0.62 eV above the ground state and the second threshold, Li $1s^22p$ $^2P^o$, which is coupled to the ^2S state by the radiation field, is only 2.47 eV above. In our opinion, such basic electronic-structure and field-free spectral characteristics allow the possibility of detailed and reliable experimentation with existing laser and detection systems. At the same time, they show clearly why the theory of multiphoton ionization must, in general, be developed and carried out beyond the single determinantal, independent-particle model. In fact, the same system was used by us a few years ago for the time-independent, many-electron many-photon computations of multiphoton detachment [15], which demonstrated distinct features due to electron-structure characteristics in initial and final states.

II. PRESENT THEORY

The conceptual framework of the approach that we have implemented for the solution of the TDSE follows the textbook prescription of expanding the time-dependent wave function in terms of field-free stationary states with time-dependent coefficients, which must be determined from the solution of the resulting system of coupled first-order differential equations. Such a strategy for solving the TDSE contains, in principle, the advantage that we can study the rate of convergence not only as a function of laser characteristics but also as a function of the free-atom (molecule) spectral characteristics, by considering systematically the effect of the number and of the type of states in the expansion [16].

The possibility of realizing the aforementioned advantage depends crucially on the availability and reliable handling of accurate wave functions for the discrete, autoionizing, and scattering states. These must contain the important effects of the self-consistent field and of interelectronic interactions. In this work, this is achieved by employing the electronic structure methods of the state-specific theory [17,18]. In this way, the initial state may be closed or open shell, ground or excited; the excited states are represented by well-optimized function spaces, and the free electron of the ionized state is represented by numerical, term-dependent, fixed-core (with polarization) Hartree-Fock (HF) scattering orbitals, thus allowing the study of properties related to the angular momenta of the scattering channels, such as partial ATI spectra and angular distribution of the photoelectron.

A. Choice of the interaction operator

The aim is to solve the TDSE

$$i\frac{d}{dt}|\Psi(\mathbf{r},t)\rangle = H_{\text{tot}}(t)|\Psi(\mathbf{r},t)\rangle \ , \tag{1}$$

where the time-dependent wave function $\Psi(\mathbf{r},t)$ contains the information of the time evolution of the initial atomic state due to its interaction with a pulsed laser field. In the semiclassical dipole approximation, the total Hamiltonian $H_{\text{tot}}(t)$ is written as

$$H_{\text{tot}}(t) = H_{\text{at}} + H_{\text{int}}(t) \ , \tag{2}$$

where H_{at} is the field-free atomic Hamiltonian.

Without posing any restrictions on the general form of Eq. (2), we have chosen the interaction Hamiltonian to be in the velocity form, for reasons of convenient evaluation of continuum-continuum dipole integrals with numerical functions (Appendix A). Thus

$$H_{\text{int}}(t) = i\,\mathbf{A}(t)\cdot\nabla + \tfrac{1}{2}A^2(t) \tag{3a}$$

with (single-frequency case)

$$\mathbf{E}(t) = -\frac{d}{dt}\mathbf{A}(t) = \mathbf{E}_0 f(t)\sin(\omega t) \ , \tag{3b}$$

where the vector potential $\mathbf{A}(t)$ contains the information about the laser frequency (ω), intensity $(\sim E_0^2)$, and temporal pulse shape $[f(t)]$. The second term, $\tfrac{1}{2}A^2(t)$ in expression (3a), can be neglected, since it is just a phase factor of the time-dependent wave function $\Psi(\mathbf{r},t)$.

The gauge-invariant formulation of the interaction of electromagnetic radiation with matter [19] shows that the expansion coefficients of the field-free atomic states cannot be interpreted as probability amplitudes [20]. This is in contrast to the case of the length form

$$H_{\text{int}}(t) = -\mathbf{r}\cdot\mathbf{E}(t) \ , \tag{3c}$$

where the aforementioned expansion coefficients can indeed be interpreted as probability amplitudes. Hence, in the velocity form of the interaction [Eq. (3a)], it is the expansion coefficients of a new function $\Psi'(\mathbf{r},t)$,

$$\Psi'(\mathbf{r},t)=e^{-i\,\mathbf{A}(t)\cdot\mathbf{r}}\Psi(\mathbf{r},t) \ , \tag{3d}$$

which are to be interpreted as probability amplitudes [20,21]. In addition, when using the "preferential gauge" [22], which implies a vanishing vector potential $\mathbf{A}(t)$ whenever the electromagnetic field becomes zero, the choice of a field-free atomic state for $t=0$ is valid. Keeping in mind the above interpretation of the expansion coefficients of $\Psi'(\mathbf{r},t)$, the use of the velocity form has the important advantage that it allows a convenient numerical treatment of the singular part of the continuum-continuum dipole moment matrix elements (see the following subsection).

B. The solution of the TDSE and the calculation of observables

We expand the time-dependent wave function of Eq. (1) in the N-electron set of the field-free states of the atom [16]

$$|\Psi(\mathbf{r},t)\rangle = \sum_{i,n} \alpha_i(n,t)|i,n\rangle + \sum_i \int b_i(E,t)|i,E\rangle dE \ , \tag{4}$$

where $|i,n\rangle$ are the atomic bound states plus the multiply excited states (autoionizing states) and $|i,E\rangle$ are the energy normalized continuum wave functions, where the index i runs over the different channels. Substituting Eq. (4) into Eq. (1) results in the system of coupled integro-differential equations

$$i\frac{d}{dt}\alpha_i(n,t)=\varepsilon_{i,n}\alpha_i(n,t)+iA(t)\sum_{j,m}B_{ij}(n,m)\alpha_j(m,t)$$
$$+iA(t)\sum_j \int b_j(E,t)D_{ij}(n,E)dE \ ,$$

$$i\frac{d}{dt}b_i(E,t)=Eb_i(E,t)+iA(t)\sum_{j,m}D_{ij}(E,m)\alpha_j(m,t)$$
$$+iA(t)\sum_j \int b_j(E',t)C_{ij}(E,E')dE' \ , \tag{5}$$

where $\varepsilon_{i,n}$ are the calculated energies of the bound and, if necessary, of the multiply excited states of the atom, $B_{ij}(n,m)$ is the bound-bound dipole matrix element, $D_{ij}(n,E)$ is the bound-continuum dipole matrix element, and $C_{ij}(E',E)$ is the continuum-continuum dipole matrix element.

From the accumulated knowledge in the field of computation of wave functions and properties of polyelectronic atoms, it can be deduced that solving the system of equations (5) reliably is a very demanding problem, even if supercomputers are available. It turns out that the use of state-specific wave functions for the discrete or the continuous spectrum [17,18] allows the incorporation of the important information while keeping the overall calculation manageable.

The matrix elements $B_{ij}(n,m)$ and $D_{ij}(n,E)$ are calculated numerically without any difficulty since they involve bound orbitals. On the other hand, the continuum-continuum dipole matrix elements $C_{ij}(E',E)$, which play a crucial role in the understanding of ATI, contain an on-shell singularity. For hydrogen, the exact

form of this singularity was recently studied using the known analytic functions [23]. However, for the general case of the many-electron atom, the term-dependent scattering orbitals must be obtained numerically over a large range of energies, a fact requiring the solution of a different calculational bottleneck. This has been dealt with in the following way. For $H_{\text{int}}(t)$ in the velocity form [Eq. (3a)], $C_{ij}(E',E)$ is written as (Appendix A)

$$C_{ij}(E',E)=C_{ij}^{\text{nonsingular}}(E',E)+C_{ij}^{\text{singular}}(E',E) \tag{6a}$$

with

$$C_{ij}^{\text{singular}}(E',E)=F_1(\varepsilon',\varepsilon)\delta(\varepsilon'-\varepsilon)+\mathrm{P}\frac{F_2(\varepsilon',\varepsilon)}{\varepsilon'-\varepsilon} \ , \tag{6b}$$

where P signifies the principal value. The variables ε',ε represent the positive energies of the free electrons above the thresholds of the i,j channels correspondingly. $F_1(\varepsilon',\varepsilon)$, $F_2(\varepsilon',\varepsilon)$ are well-behaved functions of the energy and of the phase shifts and are calculated numerically using the energy normalized numerical HF free-electron orbitals.

The integrals in Eq. (5) are calculated taking into account the δ function and the principal-value integration of Eq. (6b). In order to accomplish this, we choose a high-energy cutoff and the resulting energy range is associated with a mesh. The values of $b_j(E,t)$ are to be found at the mesh points. For the nonprincipal-value integrals of the system (5) this is done by the trapezoidal rule, which means that for energies between consecutive mesh points the integrand is assumed to vary linearly. For the evaluation of the principal-value integrals [Eqs. (5) and (6b)], we apply a procedure analogous to a method followed a long time ago by Altick and Moore [24]. This procedure first assumes that the well-behaved part of the integrand $[b_j(\varepsilon',t)F_2(\varepsilon,\varepsilon')]$ varies linearly with energy between consecutive mesh points and then computes the remainder of the integral exactly. The system (5) is thus reduced to a system of ordinary differential equations.

The solution of Eqs. (5) gives the time-dependent coefficients $\alpha_i(n,t)$ and $b_i(E,t)$ and subsequently any quantity of interest. For example, photoionization probabilities and rates can be deduced from the study of the quantity [25]

$$P_{\text{ion}}(t)=1-\sum|\alpha_i(n,t)|^2 \ , \tag{7}$$

where the summation in Eq. (7) concerns only the bound states of the atom. Furthermore, not only the total ATI spectrum but also partial ATI spectra are directly calculated from the $b_i(E,t)$, with

$$\frac{dP_\varepsilon(t)}{d\varepsilon}=\sum_i \frac{dP_\varepsilon^i(t)}{d\varepsilon}=\sum_i |b_i(E,t)|^2 \ , \tag{8}$$

where $dP_\varepsilon^i(t)$ is the probability that the free electron has energy between ε and $\varepsilon+d\varepsilon$ in the channel i.

Finally, higher HG can be computed by Fourier transforming the induced time-dependent dipole moment of the atomic state

$$d(t)=\langle\Psi(\mathbf{r},t)|\mathbf{d}|\Psi(\mathbf{r},t)\rangle \ , \tag{9}$$

where **d** is the dipole operator. Calculations of HG based on Eq. (9) within the model of a single active electron in a central potential have already been published by other researchers [11,26]. Our results on HG using the present state-specific approach are reported elsewhere [14].

The integration of the system of differential equations (5) has been carried out by the adaptive Bulirsch-Stöer [27] method for ordinary differential equations and by a Taylor-series expansion method (TSEM) (see Appendix B), which is based on the series expansion of the time-dependent coefficients and of the vector potential. It turns out that in most cases, the TSEM is about 5 times faster than the adaptive Bulirsch-Stöer method.

III. RESULTS FOR THE HYDROGEN ATOM

The validity of the approach of Sec. II was first checked using the exact hydrogenic wave functions of the discrete and continuous spectrum. We focused our efforts on the testing of our algorithms for the time integration of Eq. (5) and for the numerical evaluation of the on-shell continuum-continuum dipole matrix element.

The calculations were done for a laser pulse envelope $f(t)$ [Eq. (3b)] of the form

$$
f(t) = \begin{cases} \dfrac{t}{T_r}, & 0 \le t \le T_r \\[4pt] 1, & T_r \le t \le T_f \\[4pt] 1 - \dfrac{t - T_f}{T_{\text{off}}}, & T_f \le t \le T_f + T_{\text{off}} \\[4pt] 0, & t \ge T_f + T_{\text{off}}, \end{cases} \tag{10}
$$

where T_r is the time during which the pulse rises linearly, $(T_f - T_r)$ is the time interval where the pulse has constant intensity, and T_{off} is the time interval during which the pulse intensity falls to zero.

First we calculated the time evolution of hydrogen prepared in its ground state, irradiated by a laser pulse of the temporal shape (10) with frequency $\omega = 0.2$ a.u. (5.44 eV) and peak intensity $I_0 = 1.75 \times 10^{14}$ W/cm^2. T_r was equal to 10 optical cycles and T_f was equal to 30 cycles. The expansion in Eq. (4) consisted of the bound states up to principal quantum number $n = 4$ and up to angular momentum $l = 3$, of energy normalized numerical wave functions with angular momentum up to l_{max} (given below), and with an upper limit of the energy integrations in Eq. (5) equal to E_{max}. For the curves of Fig. 2, $E_{\text{max}} = 1.25$ a.u. (34.0 eV). Calculations where the upper energy integration limits were greater than 1.25 a.u. showed that the results are not significantly affected, meaning that for E_{max} of the order of a few photon energies, stable results are obtained.

The series of Figs. 2(a)–2(f) illustrate the rate of convergence of the time-dependent probability of H remaining in its ground state as a function of the number of scattering functions N_c and of angular momenta l_{max}. Once N_c or, equivalently, the energy separation ΔE is chosen, the functions $b_i(E,t)$, $D_{ij}(E,m)$, and $C_{ij}(E,E')$ are obtained and the energy integrations in Eq. (5) are done by the trapezoidal rule.

Specifically, Figs. 2(a)–2(d) refer to $l_{\text{max}} = 2$ and to N_c from 50 to 400. Stability of the results is clearly reached already at $N_c = 200$. These figures show that it is essential to ensure convergence as a function of N_c for each channel i [Eq. (5)]. Of course, by increasing N_c the size of the problem increases rapidly. For example, in order to obtain Fig. 2(a) a system of 160 differential equations had to be integrated whereas for Fig. 2(d) the number increased to 1210. In other work not presented here [14], where $n = 20$ and $l_{\text{max}} = 5$ for the bound states and $l_{\text{max}} = 20$ and $E_{\text{max}} = 70$ eV for the continuum states, the number of coupled equations reaches 27 300.

Figures 2(e) and 2(f) show results from $N_c = 200$ and $l_{\text{max}} = 3$ and 4 correspondingly. Comparing with Figs. 2(a)–2(d) we see that stable results are reached even with low angular momentum values, although the peak intensity is relatively high ($I_0 = 1.75 \times 10^{14}$ W/cm^2). This is due to the fact that the chosen frequency $\hbar\omega = 5.44$ eV does not correspond to any excited states of the discrete spectrum even after the field-induced energy shifts.

The photoionization rate, which is deduced from the linear portion of the logarithm of the time-dependent probability, was calculated to be 2.3×10^{14} sec^{-1}. This value is close to the value 2.9×10^{14} sec^{-1}, which is the outcome of the time-independent calculation of Chu and Cooper [28], and to the values 3.5×10^{14} sec^{-1} of DeVries [3] and 4.0×10^{14} sec^{-1} of Kulander [1].

The next application was the calculation of the photoionization rates of hydrogen irradiated by a laser pulse of 248 nm, a case which has been studied before [2,7]. For this wavelength, a recent experiment [29] produced absolute values for the photoionization rate for field intensities ranging from 3×10^{12} to 2×10^{14} W/cm^2. The measured rate for total electron production was less than that predicted by the earlier calculation of Chu and Cooper [28].

Our computed photoionization rates are in agreement with those of [28], (as presented in Fig. 3 of Kyrala and Nichols [29]), especially for intensities smaller than 10^{14} W/cm^2. For example, in Fig. 3, results are shown for a laser pulse of peak intensity $I_0 = 1.24 \times 10^{13}$ W/cm^2 and of temporal shape of the type of Eq. (10), with $T_r = 130$ cycles, $T_f = 215$ cycles, and $T_{\text{off}} = 45$ cycles. In particular, the probability of finding H in a bound state as a function of time is shown in Fig. 3(a), giving a photoionization rate of 1×10^{-5} a.u., which agrees with that obtained by Chu and Cooper [28] and also by us, using the time-independent complex eigenvalue Schrödinger theory of [15,30,31]. In Fig. 3(b) the ATI spectra, obtained from the probability distribution [see Eq. (8)] as a function of energy, are shown, revealing the existence of two peaks. The basis set for the results presented in Fig. 3 consisted of the bound states up to $n = 12$ and $l = 4$ and of scattering wave functions with $l_{\text{max}} = 5$, $E_{\text{max}} = 1.25$ a.u., and $N_c = 625$ energy points.

For intensities greater than 2×10^{14} W/cm^2, detailed results will be presented in the future. A sample of these results (time-consuming calculations are presently being performed) is given in Fig. 4, where the ATI spectra for $I_0 = 3.1 \times 10^{14}$ and 5.0×10^{14} W/cm^2 are presented. The
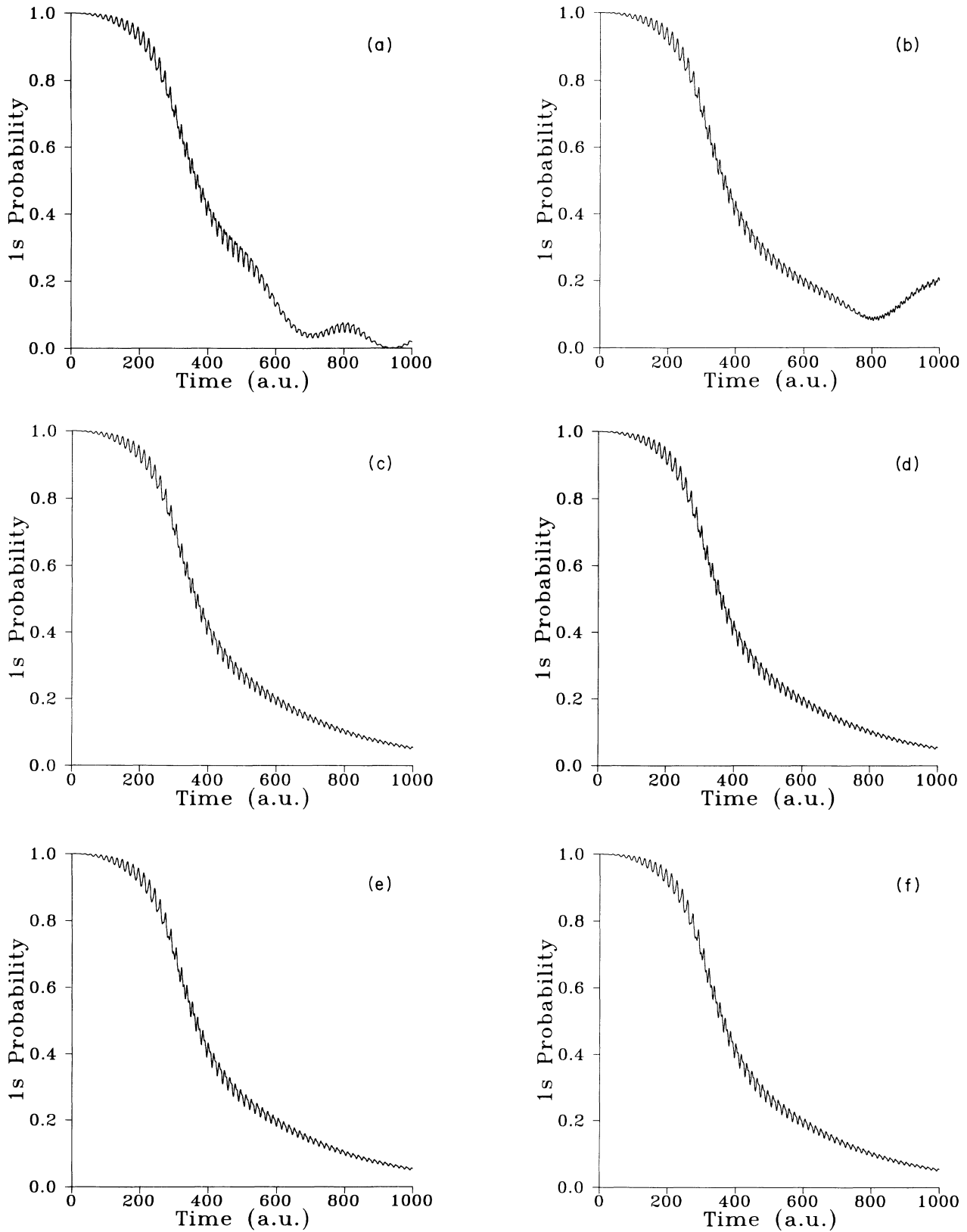
FIG. 2. Probability, as a function of time, of H remaining in its ground state for laser frequency $\omega=0.2$ a.u. and peak intensity $I_0 = 1.75 \times 10^{14}$ W/cm^2. The state-specific basis set consisted of bound states up to $n=4$ and $l=3$. (a) The continuum consisted of energy normalized scattering wave functions up to $l_{max}=2$. $N_c=50$ is the equidistant energy points with energy separation $\Delta E = 2.5 \times 10^{-2}$ a.u. (b) $l_{max}=2$, $N_c=100$, and $\Delta E = 1.25 \times 10^{-2}$ a.u. (c) $l_{max}=2$, $N_c=200$, $\Delta E = 6.25 \times 10^{-3}$ a.u. (d) $l_{max}=2$, $N_c=400$, and $\Delta E = 3.125 \times 10^{-3}$ a.u. (e) $l_{max}=3$, $N_c=200$, and $\Delta E = 6.25 \times 10^{-3}$ a.u. (f) $l_{max}=4$ $N_c=200$, and $\Delta E = 6.25 \times 10^{-3}$ a.u.

suppression of the peak corresponding to the absorption of three photons is due to the ponderomotive shift. The substructures on each peak are attributed to multiphoton ionization processes which are enhanced by excited states populated during the laser pulse. In Figs. 4(a) and 4(b) the ATI spectra for $I_0 = 3.1 \times 10^{14}$ W/cm^2 are given for two successive instants $t = 50$ and 73 cycles correspondingly, showing that, as time progresses, the substructures gradually become less important compared to the main peaks (attributed to the $1s$ ground state), while their absolute values remain essentially constant. In Fig. 4(c) the ATI spectrum for $I_0 = 5.0 \times 10^{14}$ W/cm^2 is given for $t = 29$ cycles. It is seen that with a slightly larger intensity the overwhelming population of the four-photon peak

dominates at shorter times.

Recently, LaGattuta [2] considered the ionization of hydrogen through resonant intermediate states, using a time-dependent method which belongs to the family of
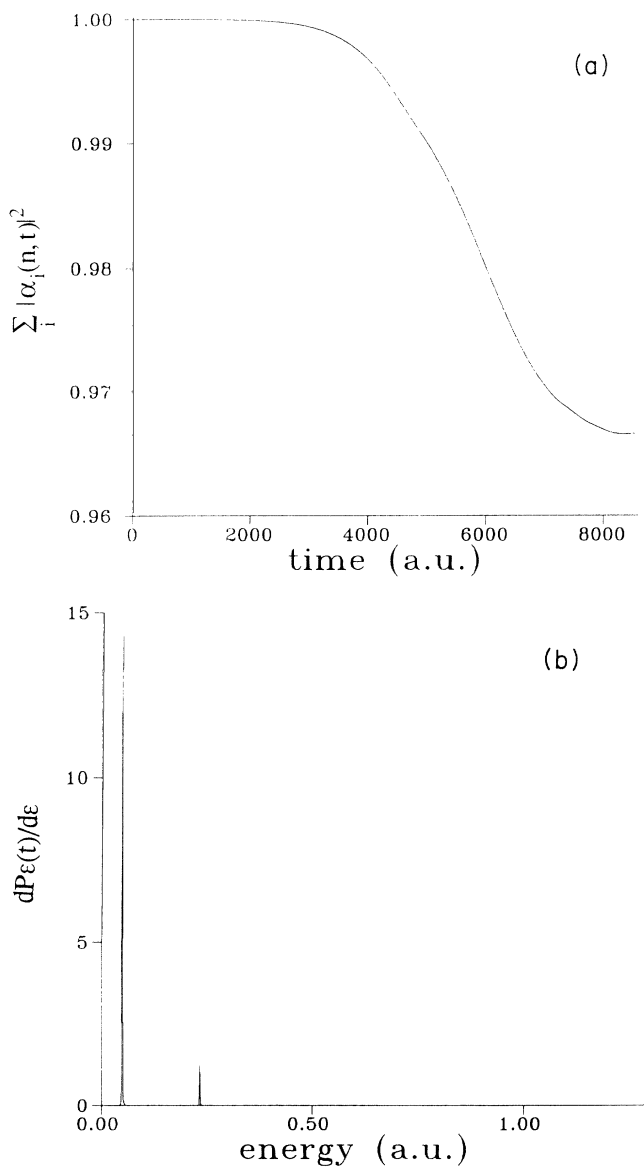
FIG. 3. (a) Time-dependent probability of finding H in any bound state, for wavelength $\lambda = 248$ nm and peak intensity $I_0 = 1.24 \times 10^{13}$ W/cm^2. (b) The corresponding ATI spectrum, at the end of the laser pulse, obtained from the probability distribution of Eq. (8).
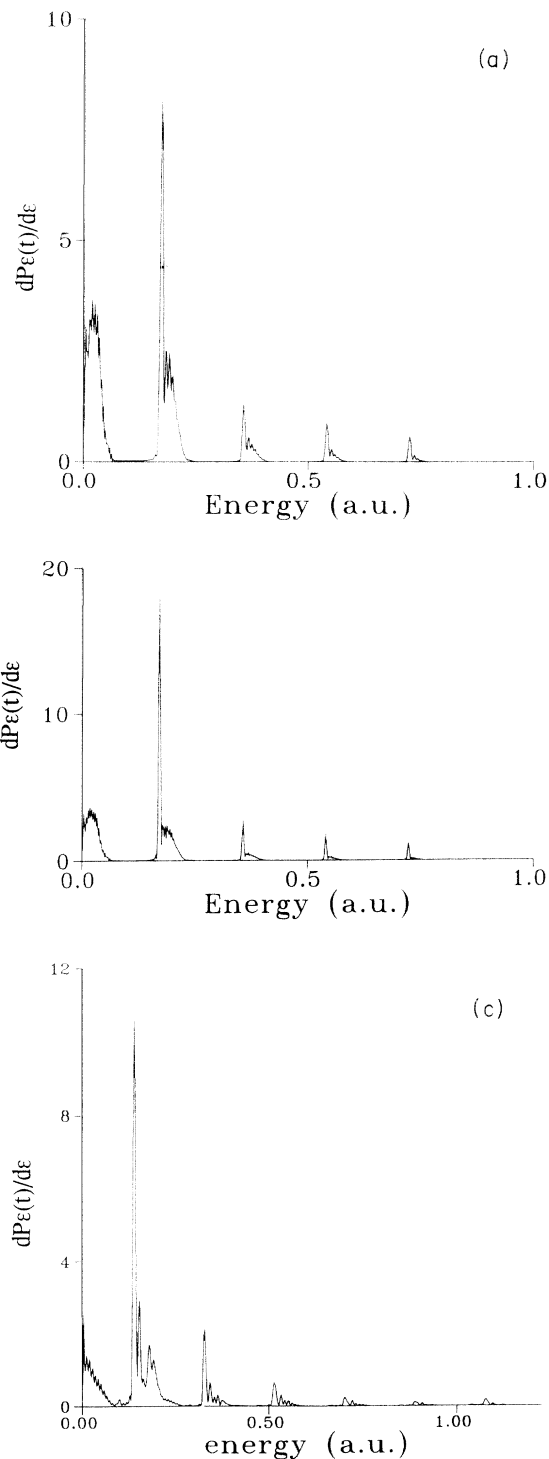
FIG. 4. ATI spectrum of H irradiated by a laser pulse of wavelength $\lambda = 248$ nm. (a) $I_0 = 3.1 \times 10^{14}$ W/cm^2 and $t = 50$ cycles. (b) $I_0 = 3.1 \times 10^{14}$ W/cm^2 and $t = 73$ cycles, (c) $I_0 = 5.0 \times 10^{14}$ W/cm^2 and $t = 29$ cycles.
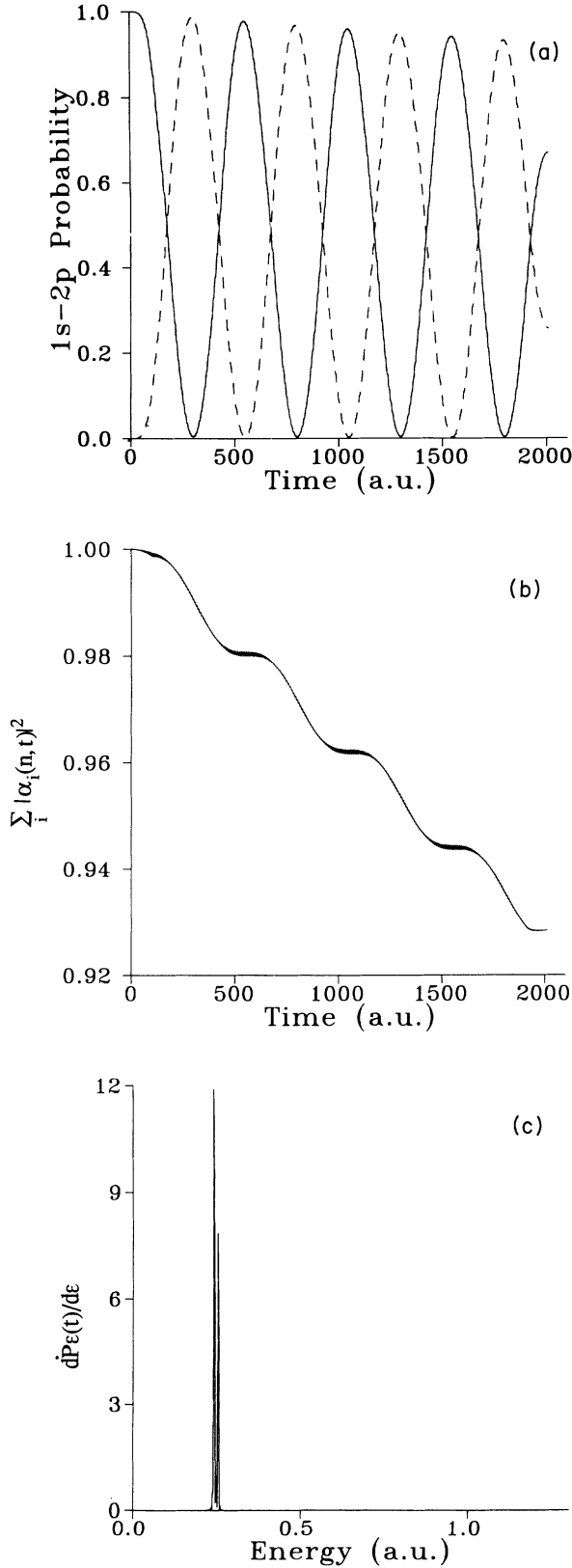
FIG. 5. H is irradiated by a laser pulse of $\omega = 0.375$ a.u. and $I_0 = 10^{13}$ W/cm^2. (a) Probability of finding H in the $1s$ (solid line) and the $2p$ (dashed line) states as a function of time. (b) Probability of finding H in any bound state as a function of time. (c) ATI spectrum at the end of the pulse.

finite-difference techniques [12]. We carried out calculations using the same parameters, i.e., a laser pulse of 50 fsec duration with peak intensity $I_0 = 10^{13}$ W/cm^2 and frequency $\omega = 0.375$ a.u. This photon frequency connects resonantly the field-free states $1s$ and $2p$. The temporal shape of the pulse is given by Eq. (10) with $T_r = 6$ cycles, $T_f = 113$ cycles, and $T_{off} = 7$ cycles. The basis functions were the same as those used to obtain Fig. 2(e). The results are shown in Fig. 5. Figure 5(a) shows the probabilities of finding H in the $1s$ (solid curve) and $2p$ (dashed curve) states as a function of time. The resonantly coupled states execute oscillations with period $T_R = 500$ a.u. This is the same value that is obtained from the definition $T_R = 2\pi/\Omega_R$, where $\Omega_R = 0.0126$ a.u. is the Rabi frequency given by $\Omega_R = \langle 1s|z|2p \rangle E_0$. In Fig. 5(b), we give the probability of finding H in any bound state as a function of time, where the Rabi oscillations between $1s$ and $2p$ are also present. By drawing the tangent to the "peaks" of the curve, a calculated ionization rate of 1.6×10^{12} sec^{-1} is obtained. This is in excellent agreement with the value 1.5×10^{12} sec^{-1} obtained in Ref. 2 and with the 2×10^{12} sec^{-1} rate obtained by our time-independent methods [15,30,31]. The ATI spectrum is shown in Fig. 5(c) where a double peak is observed, with energy separation equal to the Rabi frequency Ω_R, also in excellent agreement with the ATI spectrum of Ref. [2], Fig. 2.

IV. RESULTS FOR THE NEGATIVE ION OF Li

Figure 1 shows the part of the Li$^-$ spectrum whose time-dependent excitation was computed in this work [32]. The first photon of $\hbar\omega = 1.36$ eV opens the Li $1s^22s$ ^2S channel and the second opens the Li $1s^22p$ $^2P^o$ channel as well. These two Li states are coupled by the dipole operator.

As is well known, the wave function of the ground state Li$^-$ $1s^22s^2$ ^1S cannot be represented by a single determinant. A multiconfiguration Hartree-Fock calculation with $n = 2$ and 3 valence configurations shows immediately that the major correlation effect is that due to an angular correlation $2s^2 \leftrightarrow 2p^2$ and, only to a lesser degree, to a radial correlation $2s^2 \leftrightarrow 3s^2$. This fact has led us to the choice of the two-term wave function for the ground state

$$\Phi_0^{MCHF} = 0.933 \ 1s^22s^2 + 0.360 \ 1s^22p^2 \ . \tag{11}$$

The above electronic structure features imply immediately that the physics of the interaction of the Li$^-$ ^1S state with a strong laser pulse ought to be analyzed and computed at a level beyond the independent-particle model. In other words, the computations ought to account for the major electron correlation effect in the initial state Φ_0 and for the open-shell, multichannel character of the final states $1s^22s\varepsilon l$ and $1s^22p\varepsilon'l$, represented by Hartree-Fock wave functions. Then, the time evolution of Li$^-$ for photon absorption as shown in Fig. 1 is driven by the coupling of Φ_0 to the continuum states with free-electron energies ε and ε'

$$\Phi_1(L;E) = 1s_1^2 2s_1 \varepsilon l \ ^1L, \quad L = S, P, D \tag{12a}$$

$$\Phi_2(l,L;E) = 1s_2^2 2p_2 \varepsilon' l \; ^1L, \quad L = |l-1|, \dots, l+1 \; . \quad (12b)$$

The indices 1 and 2 indicate the state specific character of the HF orbitals. The free-electron orbitals $\varepsilon l, \varepsilon' l$ are obtained numerically by solving the term-dependent fixed core (with polarization), HF equations.

By combining Eqs. (4), (11), (12a), and (12b), the time-dependent wave function is written as

$$\Psi(t) = \alpha_0(t)\Phi_0 + \sum_{L=0}^{L_1} \int_0^\infty \beta_{1,L}(\varepsilon,t)\Phi_1(L;E_1+\varepsilon)d\varepsilon$$

$$+ \sum_{l=0}^{L_2} \left[\sum_{L=|l-1|}^{l+1} \int_0^\infty \beta_{2,l,L}(\varepsilon,t)\Phi_2(l,L;E_2+\varepsilon)d\varepsilon \right] .$$

$$(13)$$

E_1, E_2 are the energies of the first and second Li channels, respectively, with values shown in Fig. 1. The laser pulse has the temporal shape (10) with $T_r = 5$ cycles, $T_f = 15$ cycles, and $T_{\text{off}} = 0$ cycles. This choice was made after trial calculations showed that in this way saturation phenomena are minimized. For frequency $\omega = 1.36$ eV (0.05 a.u.) and peak intensity $I_0 = 7 \times 10^{10}$ W/cm^2, we found convergent results for $L_1 = 2 = L_2$ [see Eqs. (13), (12a), and (12b)]. The bound-continuum matrix elements have the form

$$\langle \Phi_0|H_{\text{int}}|1s_1^2 2s_1 \varepsilon p \; ^1P^o \rangle$$

$$= c_1\sqrt{2}\langle 1s|1s_1\rangle^2 \langle 2s|2s_1\rangle \langle 2s|H_{\text{int}}|\varepsilon p\rangle$$

$$+ c_2(-\sqrt{\tfrac{6}{3}})\langle 1s|1s_1\rangle^2 \langle 2p|\varepsilon p\rangle \langle 2p|H_{\text{int}}|2s_1\rangle \; ,$$

$$(14a)$$

$$\langle \Phi_0|H_{\text{int}}|1s_2^2 2p_2 \varepsilon s \; ^1P^0 \rangle$$

$$= c_1\sqrt{2}\langle 1s|1s_2\rangle^2 \langle 2s|\varepsilon s\rangle \langle 2s|H_{\text{int}}|2p_2\rangle$$

$$+ c_2(-\sqrt{\tfrac{6}{3}})\langle 1s|1s_2\rangle^2 \langle 2p|2p_2\rangle \langle 2p|H_{\text{int}}|\varepsilon s\rangle \; ,$$

$$(14b)$$

$$\langle \Phi_0|H_{\text{int}}|1s_2^2 2p_2 \varepsilon d \; ^1P^0 \rangle$$

$$= c_2(\tfrac{2}{3})\langle 1s|1s_2\rangle^2 \langle 2p|2p_2\rangle[-iA_z(t)]\langle 2p|Q|\varepsilon d\rangle \; ,$$

$$(14c)$$

where the operator Q is defined in Appendix A and the values of c_1, c_2 are given in Eq. (11). The overlaps and one-body integrals contained in Eqs. (14) are calculated numerically.

As an illustrative example, we give two types of continuum-continuum dipole moment matrix elements:

$$\langle 1s_1^2 2s_1 \varepsilon s_1 \; ^1S|H_{\text{int}}|1s_1^2 2s_1 \varepsilon p_1 \; ^1P^o \rangle = \langle \varepsilon s_1|H_{\text{int}}|\varepsilon p_1\rangle \; ,$$

$$(15a)$$

$$\langle 1s_1^2 2s_1 \varepsilon s_1 \; ^1S|H_{\text{int}}|1s_2^2 2p_2 \varepsilon s_2 \; ^1P^o \rangle$$

$$= \langle 1s_1|1s_2\rangle^2 \langle \varepsilon s_1|\varepsilon s_2\rangle \langle 2s_1|H_{\text{int}}|2p_2\rangle$$

$$+ \langle 1s_1|1s_2\rangle^2 \langle 2s_1|\varepsilon s_2\rangle \langle \varepsilon s_1|H_{\text{int}}|2p_2\rangle \; . \quad (15b)$$

The matrix element in Eq. (15a) is evaluated by the method developed in Appendix A applied to negative ions [effective charge $Z=0$ in Eq. (A4)]. The same method is used for the computation of the singularity of the overlap $\langle \varepsilon s_1|\varepsilon s_2\rangle$ in Eq. (15b).

The integrals in the coupled equations were performed as explained in Sec. II B, by choosing a high-energy limit of 0.36 a.u., with energy separation 5×10^{-4} a.u. between consecutive mesh points. The resulting system of ordinary differential equations is of the order of 6000 equations.

In addition to the final-state effect through the field-induced coupling of the two channels, an important question that we wanted to answer is the following: How do the effects of electronic structure and of electron correlation manifest themselves as a function of field intensity on phenomena such as ATI? For example, in Fig. 1 it is seen that for the first photon the $1s^2 2p \; ^2P^o$ channel is closed. This is the channel that is directly connected with the correlation correction $1s^2 2p^2$ of the ground state as a virtual dipole transition. It would then be interesting to check its influence on the overall ATI process as a function of intensity.

Figure 6(a) shows that ATI spectrum for $I_0 = 7 \times 10^{10}$ W/cm^2 and $\hbar\omega = 1.36$ eV, obtained from Eqs. (8) and (13) at $t = 15$ cycles as

$$\frac{dP_\varepsilon(t)}{d\varepsilon} = \sum_{L=0}^{L_1} |\beta_{1,L}(\varepsilon,t)|^2$$

$$+ \sum_{l=0}^{L_2} \left[\sum_{L=|l-1|}^{l+1} |\beta_{2,l,L}(\varepsilon,t)|^2 \right] . \quad (16)$$

A series of peaks appear that are not separated by the photon energy ω. This fact is explained in Figs. 6(b) and 6(c). Figure 6(b) shows the partial ATI spectrum for the first detachment threshold, given by the first term of the right-hand side of Eq. (16). Two peaks separated by photon energy ω appear, where the first peak is located at the energy $\omega - |E_1 - E_0|$ since the ponderomotive shift is not appreciable. Figure 6(c), where the abscissa has a different scale, shows the partial ATI spectrum for the second detachment threshold, given by the second term on the right-hand side of Eq. (16). Three peaks are observed with the distance between the first and the third peak being ω. The first peak corresponds to the absorption of two photons and is located at $2\omega - |E_2 - E_0|$. The second peak is the signature of the field-induced interchannel coupling [see, for example, Eq. (15b)]. The position of this peak corresponds exactly to the position of the first peak of the partial ATI of Fig. 6(b). The third peak of Fig. 6(c) is due to two-photon absorption and refers to the second threshold. Because of the different scales, it almost disappears in the full spectrum of Fig. 6(a). These features are not expected to change by the free Hamiltonian interchannel coupling, since this only leads to some redistribution of the probabilities in the final state which is independent of the field intensity.

In Fig. 7(a) the ATI spectrum is shown for $\omega = 0.05$

a.u., peak intensity $I_0 = 1.12 \times 10^{12}$ W/cm^2, and $t = 7$ cycles. Figure 7(b) shows the same spectrum, but now the initial state is considered to be represented by a single configuration function. The fourth peak, which corresponds to the absorption of two photons above the first detachment threshold, is now considerably lower. This means that the correlation in the initial state can have an observable effect on the final-state probability distribution through the dipole coupling

$1s^2 2p^2 \underset{\hbar\omega}{\leftrightarrow} 1s_2^2 2p_2 \varepsilon d \underset{\hbar\omega}{\leftrightarrow} 1s_1^2 2s_1 \varepsilon' d$. Also, the third peak, which corresponds to the absorption of two photons above the second detachment threshold, seems to be larger due to the presence of correlation in the initial state. The fifth peak in Fig. 7(a), which corresponds to the absorption of three photons above the second detachment threshold, is also attributable to initial-state correlation.
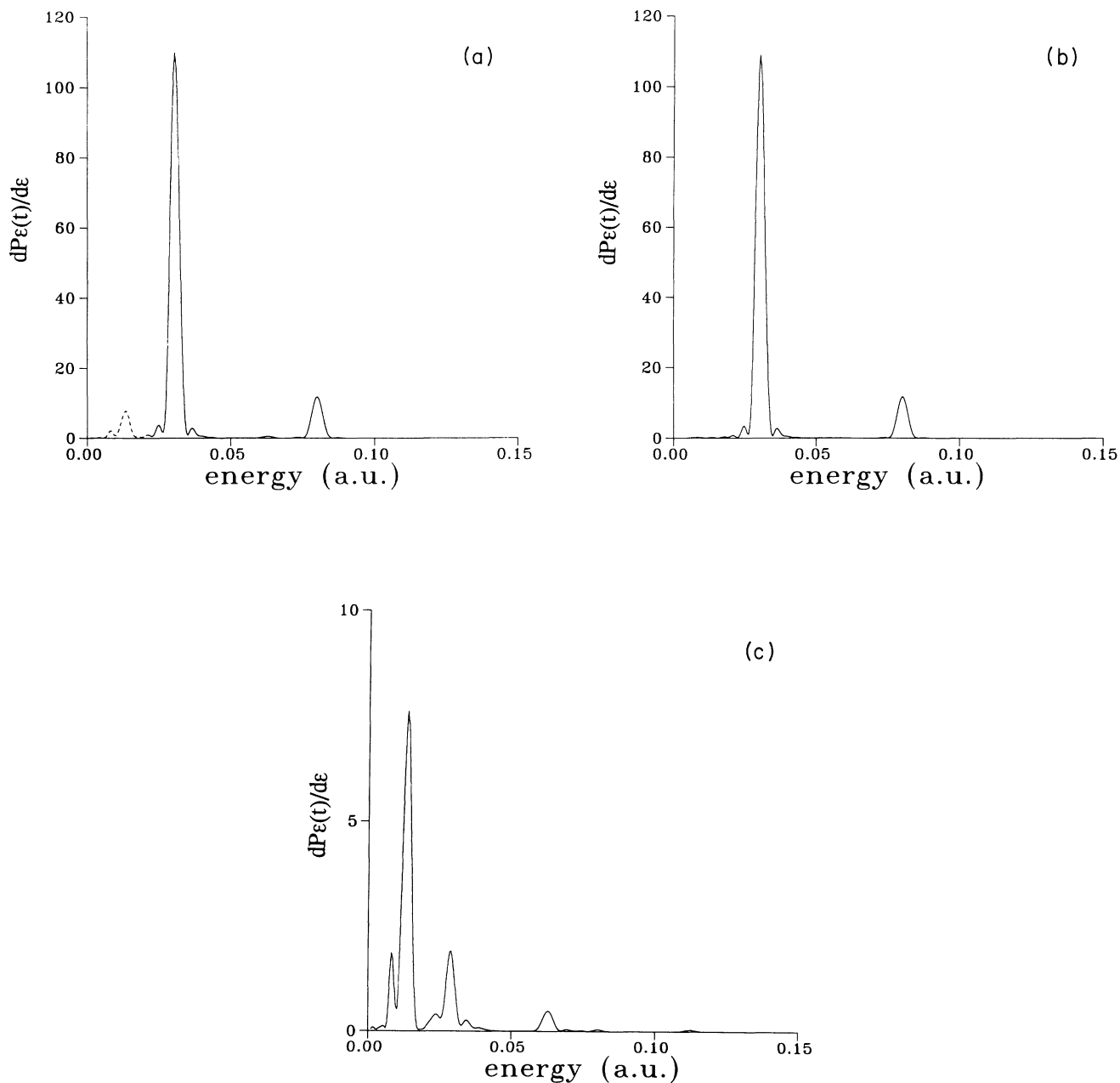
FIG. 6. ATI spectra of Li$^-$ irradiated by a laser pulse of frequency $\omega = 1.36$ eV and peak intensity $I_0 = 7 \times 10^{10}$ W/cm^2 at $t = 15$ cycles. (a) Total ATI spectrum. Solid line, peaks corresponding to the first threshold; dashed line, peaks corresponding to the second threshold. (b) Partial ATI above the first detachment threshold. (c) Partial ATI above the second detachment threshold.
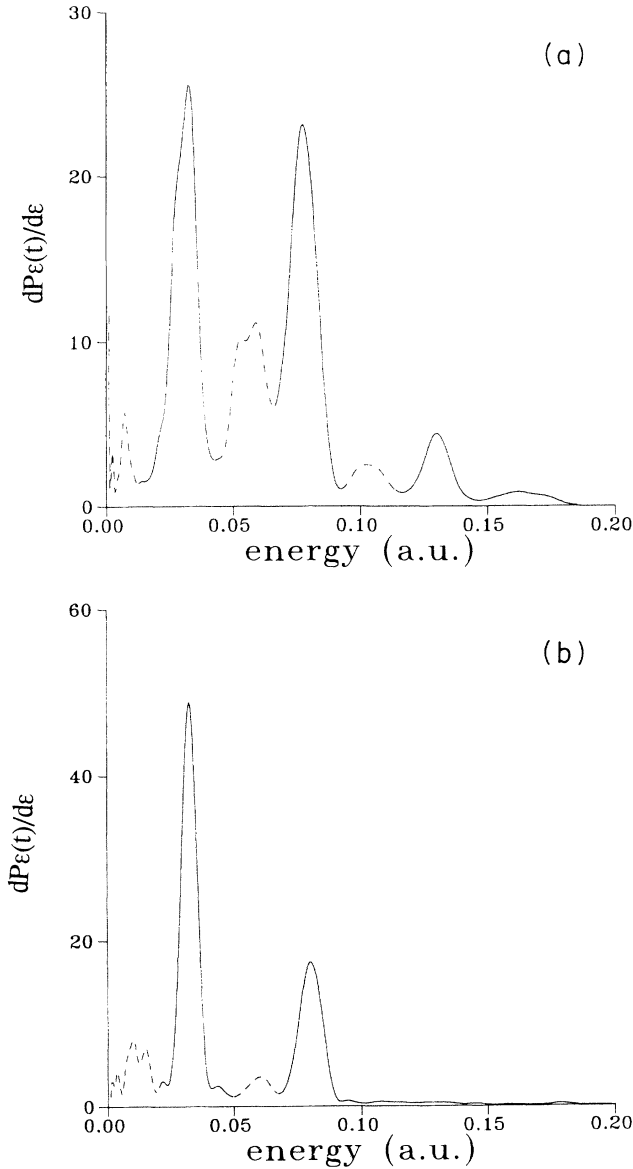
FIG. 7. ATI spectra of Li$^-$ irradiated by a laser peak of $\omega=1.36$ eV and $I_0=1.12\times10^{12}$ W/cm^2 at $t=7$ cycles. (a) The initial-state wave function contains the $1s^22p^2$ correlation configuration. (b) The initial-state wave function is represented by the HF function only. Solid line, peaks corresponding to the first threshold; dashed line, peaks corresponding to the second threshold.

V. CONCLUSION

We have presented a theory and computational method for the *ab initio* calculation of the response of a polyelectronic atomic state, ground or excited, to a short pulse of laser radiation. This is done by solving the TDSE in terms of state-specific discrete, autoionizing, and scattering wave functions $\Phi_{n,E}$, comprising the expansion of $\Psi(\mathbf{r},t)$ [Eq. (4)]. In order to compute the continuum-continuum dipole interaction matrix elements with numerical functions, we developed the method of Appendix A. Also, the efficient solution of the system of

thousands of coupled differential equations of the type of Eq. (5) is done by the method of Appendix B. The testing of the methods was done on the H atom where the exact wave functions were used in numerical form.

The present approach allows the possibility of understanding the strong laser-atom interaction in terms of the details of the electronic structure of each state contributing to the time evolution of the system. For example, we showed that the negative ion (Li$^-$) ATI spectra are affected as a function of intensity by strong ground-state angular correlations which are combined with a closely lying open channel of the continuum. Obviously, for polyelectronic neutral atoms, intermediate discrete levels as well as multiply excited autoionizing states can easily be incorporated into expansion (4) allowing detailed studies of their effect on observables. This topic will be the subject of a future publication.

APPENDIX A: THE FREE-FREE TRANSITION MATRIX ELEMENT (VELOCITY FORM)

The continuum-continuum dipole matrix element $C_{ij}(E',E)$ is defined as

$$C_{ij}(E,E')=\langle i,E|Q|j,E'\rangle \tag{A1}$$

with

$$|i,E\rangle=\mathcal{A}(\Phi_i^{(N-1)}\otimes u_{\varepsilon l}) . \tag{A2}$$

Here $\mathcal{A}$ is the antisymmetrizer, $\Phi_i^{(N-1)}$ represents the $(N-1)$-electron core wave function defining the channel i, and $u_{\varepsilon l}$ is the free-electron orbital with angular momentum l and positive energy ε. The dipole moment operator Q is explicitly given below [Eq. (A5)]. The matrix element of Eq. (A1) is separated into two parts: (a) the nonsingular $C_{ij}^{\text{nonsingular}}(E,E')$, which includes dipole matrix elements containing a bound and a continuum orbital (this part presents no numerical difficulties) and (b) the singular

$$C_{ij}^{\text{singular}}(E,E')=\langle \Phi_i^{(N-1)}|\Phi_j^{(N-1)}\rangle\langle u_{\varepsilon l}|Q|u_{\varepsilon'l'}\rangle , \tag{A3a}$$

which refers to dipole matrix elements containing two continuum orbitals. The singularity comes from the free-free transition matrix element $\langle u_{\varepsilon l}|Q|u_{\varepsilon'l'}\rangle$ and specifically from the contribution to this matrix element of the asymptotic part of the free orbitals. We note that the $u_{\varepsilon l}$ are represented up to their asymptotic region, by numerical, term-dependent, fixed-core Hartree-Fock scattering orbitals. Thus the singular dipole matrix element is also separated into two parts: the nonasymptotic, which is calculated numerically without any difficulty, and the asymptotic, which can be treated analytically giving the correct behavior around the singularity. We write accordingly

$$\langle u_{\varepsilon l}|Q|u_{\varepsilon'l'}\rangle=\int_0^\infty u_{\varepsilon l}Qu_{\varepsilon'l'}dr$$

$$=\int_0^{R_c} u_{\varepsilon l}Qu_{\varepsilon'l'}dr+\int_{R_c}^\infty u_{\varepsilon l}Qu_{\varepsilon'l'}dr . \tag{A3b}$$

Consider an electron moving in the field of an ion (atom). For a sufficiently large radius R_c, the short-range potentials become negligible and the Hamiltonian assumes the

hydrogenlike (or empty space) form. Thus, in the region $R > R_c$, the one-electron wave functions $u_{\varepsilon l}$ are linear combinations of the Coulomb (or Bessel) regular and irregular functions, satisfying the equation

$$hu_{\varepsilon l} \equiv \left[-\frac{1}{2}\frac{d^2}{dr^2} + \frac{l(l+1)}{2r^2} - \frac{Z}{r} \right] u_{\varepsilon l} = \varepsilon u_{\varepsilon l} , \quad (A4)$$

where the effective charge Z is zero for a neutral atom. The velocity form of the dipole operator

$$Q = \frac{d}{dr} + \frac{C}{2r} , \quad (A5)$$

where $C = l'(l'+1) - l(l+1)$, is used for the calculation of the free-free transition matrix elements and $|l'-l| = 1$. In order to calculate these matrix elements numerically, we transform to the acceleration form of the dipole operator. This is achieved through the use of the "commutator" relation

$$[Qh' - hQ] = \frac{Z}{r^2} , \quad (A6)$$

where h' is the Hamiltonian (A4) with angular momentum l'. Integrating the above relation by parts, one has [33]

$$\int_{R_c}^{R} u_{\varepsilon l}(Qh' - hQ)u_{\varepsilon' l'} dr = (\varepsilon' - \varepsilon)\int_{R_c}^{R} u_{\varepsilon l} Q u_{\varepsilon' l'} dr$$
$$+ F_{\varepsilon\varepsilon'}(R) - F_{\varepsilon\varepsilon'}(R_c) , \quad (A7)$$

where

$$F_{\varepsilon\varepsilon'}(R) = \frac{1}{2} u_{\varepsilon l}\frac{d^2}{dr^2} u_{\varepsilon' l'} - \frac{1}{2}\frac{d}{dr} u_{\varepsilon l}\frac{d}{dr} u_{\varepsilon' l'}$$
$$+ \frac{C}{4R}\left[u_{\varepsilon l}\frac{d}{dr} u_{\varepsilon' l'} - u_{\varepsilon' l'}\frac{d}{dr} u_{\varepsilon l} \right]$$
$$- \frac{C}{4R^2} u_{\varepsilon l} u_{\varepsilon' l'} . \quad (A8)$$

Setting

$$W_{\varepsilon\varepsilon'}(R, R_c) = \int_{R_c}^{R} u_{\varepsilon l}\frac{Z}{r^2} u_{\varepsilon' l'} dr \quad (A9)$$

and making use of (A6), Eq. (A7) is written as

$$\int_{R_c}^{R} u_{\varepsilon l} Q u_{\varepsilon' l'} dr = \frac{1}{\varepsilon' - \varepsilon}[W_{\varepsilon\varepsilon'}(R, R_c) + F_{\varepsilon\varepsilon'}(R_c)]$$
$$- \frac{1}{\varepsilon' - \varepsilon} F_{\varepsilon\varepsilon'}(R) . \quad (A10)$$

The limit of the above expression for $R \to \infty$ is to be taken. For the last term in (A10), this is a delicate operation [34]. Substituting the asymptotic form of the Coulomb wave function

$$u_{\varepsilon l} \to \left[\frac{2}{\pi k} \right]^{1/2} \sin\left[kR + n\ln(2kR) + \sigma_l + \delta_l - l\frac{\pi}{2} \right]$$

$[k = \sqrt{2\varepsilon}, \quad n = Z/k, \quad \sigma_l(n) = \arg\Gamma(l+1+in)$ is the Coulomb, and δ_l is the additional phase shift], in the definition of $F_{\varepsilon\varepsilon'}(R)$ Eq. (A8), one obtains

$$\frac{1}{\varepsilon' - \varepsilon} F_{\varepsilon\varepsilon'}(R) \to \mathrm{sgn}(l'-l)\frac{k'}{\pi\sqrt{kk'}}\frac{1}{k'-k}\sin[(k-k')R + \sigma_l + \delta_l - \sigma_{l'} - \delta_{l'}]$$
$$- \mathrm{sgn}(l'-l)\frac{k'}{\pi\sqrt{kk'}}\frac{1}{k'+k}\sin[(k'+k)R + \sigma_l + \delta_l + \sigma_{l'} + \delta_{l'}] . \quad (A11)$$

Making use of the formulas

$$\lim_{R \to \infty}\frac{1}{\pi}\frac{\sin Rx}{x} = \delta(x) , \quad (A12a)$$

$$\lim_{R \to \infty}\frac{1 - \cos Rx}{x} = \mathrm{P}\frac{1}{x} , \quad (A12b)$$

where P denotes principal-value integration, one realizes that the contribution of the second term in (A11) is zero since the wave vector is a positive quantity. In order to apply Eq. (A12b) one must note that for equal energies, Eq. (A7) gives

$$W_{\varepsilon\varepsilon}(R, R_c) + F_{\varepsilon\varepsilon}(R_c) = F_{\varepsilon\varepsilon}(R) , \quad (A13)$$

where

$$F_{\varepsilon\varepsilon}(R) = \mathrm{sgn}(l'-l)\frac{k}{\pi}\sin(\sigma_l + \delta_l - \sigma_{l'} - \delta_{l'}) . \quad (A14)$$

Thus we obtain

$$\int_{R_c}^{\infty} u_{\varepsilon l} Q u_{\varepsilon' l'} dr$$
$$= \mathrm{P}\frac{1}{\varepsilon' - \varepsilon}[W_{\varepsilon\varepsilon'}(\infty, R_c) + F_{\varepsilon\varepsilon'}(R_c)]$$
$$+ \mathrm{sgn}(l'-l)\cos(\sigma_l + \delta_l - \sigma_{l'} - \delta_{l'})\sqrt{2\varepsilon}\delta(\varepsilon - \varepsilon') . \quad (A15)$$

Now we are able to define the functions $F_1(\varepsilon', \varepsilon), F_2(\varepsilon', \varepsilon)$, which are the constituents [see Eq. (6b) in the text] of the singular part of the free-free transition matrix element. This is done by combining Eqs. (6b), (A3b), and (A15), obtaining finally

$$F_1(\varepsilon', \varepsilon) = \mathrm{sgn}(l'-l)\cos(\sigma_l + \delta_l - \sigma_{l'} - \delta_{l'})\sqrt{2\varepsilon} ,$$
$$F_2(\varepsilon', \varepsilon) = W_{\varepsilon\varepsilon'}(\infty, R_c) + F_{\varepsilon\varepsilon'}(R_c)$$
$$+ (\varepsilon' - \varepsilon)\int_0^{R_c} u_{\varepsilon l} Q u_{\varepsilon' l'} dr . \quad (A16)$$

The quantity $W_{\varepsilon\varepsilon'}(\infty, R_c)$, which was defined in (A9), is evaluated by considering that for $r > R_c$ the WKB ap-

proximation is valid [35]. This permits the execution of an alternative numerical technique using asymptotic expansions [36]. In the case of hydrogen, where the function $F_2(\varepsilon', \varepsilon)$ is given as

$$F_2(\varepsilon', \varepsilon) = W_{\varepsilon', \varepsilon}(\infty, 0)$$

$$= \int_0^{R_c} u_{\varepsilon l} \frac{Z}{r^2} u_{\varepsilon' l} dr + \int_{R_c}^{\infty} u_{\varepsilon l} \frac{Z}{r^2} u_{\varepsilon' l} dr \ , \qquad (A17)$$

the first term on the right-hand side of (A17) is evaluated numerically.

APPENDIX B:
TAYLOR-SERIES EXPANSION METHOD

The time integration of the system of coupled differential equations of the type of Eq. (5) is done as follows. As already mentioned in the text, the integrals which appear in Eq. (5) are performed using the trapezoidal rule. The result of this integration is the transformation of Eq. (5) into the following numerical problem:

$$i \frac{d}{dt} \mathbf{x}(t) = [A + F(t)B] \mathbf{x}(t) \ , \qquad (B1)$$

where $\mathbf{x}(t)$ is the vector of the unknown time-dependent coefficients $\alpha_i(n, t)$ and $b_i(E, t)$, A is the matrix representation of the free-atom Hamiltonian in the basis set of Eq. (4), B is the matrix representation of the dipole operator in the basis set of Eq. (4), and $F(t)$ is the time-dependent vector potential $A(t)$ or electric field $E(t)$ [Eqs. (3a)–3(c)], which contains the information about the laser pulse.

Suppose that the vector $\mathbf{x}(t)$ is known for a time instant t_0. Then the vector $\mathbf{x}(t)$ for $t = t_0 + \Delta t$ is given by expanding $\mathbf{x}(t)$ in a Taylor series around t_0

$$\mathbf{x}(t) = \sum_{n=0} \mathbf{x}^{(n)}(t_0) \frac{(\Delta t)^n}{n!} \ , \qquad (B2)$$

where $\mathbf{x}^{(n)}(t_0)$ is the nth derivative of $\mathbf{x}(t)$ for $t = t_0$ and

$$\mathbf{x}^{(0)}(t_0) = \mathbf{x}(t_0) \ . \qquad (B3)$$

If we had a way of calculating $\mathbf{x}^{(n)}(t_0)$, then the solution $\mathbf{x}(t)$ would be obtained by performing the summation of Eq. (B2) up to $n = N$. The Nth (last) term of the summation (B2) should then satisfy the condition

$$\max \left| \mathbf{x}^{(N)}(t_0) \frac{(\Delta t)^N}{N!} \right| < \varepsilon \ , \qquad (B4)$$

where max means that we consider the coefficient of the vector in parentheses which has the maximum absolute value. The quantity ε is a very small positive number, which also determines the accuracy of the summation (B2). Also, the smaller the number ε, the larger the integer N [denoting the last term of the summation (B2)] [37].

The calculation of $\mathbf{x}^{(n)}(t_0)$ can be done by substituting Eq. (B2) into Eq. (B1), and by using two expansions

$$\frac{d}{dt} \mathbf{x}(t) = \sum_{n=0} \mathbf{x}^{(n+1)}(t_0) \frac{(\Delta t)^n}{n!} \qquad (B5)$$

and

$$F(t) = \sum_{n=0} F^{(n)}(t_0) \frac{(\Delta t)^n}{n!} \ . \qquad (B6)$$

The result of the above operations, after some algebra, is

$$\frac{1}{(n+1)!} \mathbf{x}^{(n+1)}(t_0)$$

$$= -i \frac{1}{n+1} A \left[\frac{1}{n!} \mathbf{x}^{(n)}(t_0) \right]$$

$$- i \frac{1}{n+1} B \sum_{m=0}^{n} \frac{F^{(n-m)}(t_0)}{(n-m)!} \left[\frac{1}{m!} \mathbf{x}^{(m)}(t_0) \right] \ ,$$

$$n = 0, 1, 2, \ldots . \qquad (B7)$$

The recursion formula (B7) permits the calculation of the derivatives, at any order, of the vector $\mathbf{x}(t)$ as shown below:

from $\mathbf{x}^{(0)}(t_0) = \mathbf{x}(t_0)$ we obtain $\mathbf{x}^{(1)}(t_0)$,

from $\mathbf{x}^{(0)}(t_0), \mathbf{x}^{(1)}(t_0)$ we obtain $\mathbf{x}^{(2)}(t_0)$,

$$\vdots \qquad\qquad \vdots$$

from $\mathbf{x}^{(0)}(t_0), \mathbf{x}^{(1)}(t_0), \ldots, \mathbf{x}^{(n-1)}(t_0)$ we obtain $\mathbf{x}^{(n)}(t_0)$.

The above process is terminated at the point where the condition (B4) is satisfied. Then we assume that we have found the solution of Eq. (B1) at a next time t, within the accuracy imposed by (B4).

In practice, we consider that the new time $t = t_0 + \Delta t$ coincides with the next t_0 and that the procedure from Eqs. (B1)–(B7) starts again. We note that the solution given by Eq. (B2) is analytic, meaning that we can find $\mathbf{x}(t)$ at any value of t between t_0 and $t_0 + \Delta t$ without starting the procedure described above. This is important when, for example, we wish to study high harmonic generation [Eq. (9) in the text] since, without additional computational effort, we can find the induced dipole moment $d(t)$ at any number of time instants. The square of the Fourier transform of $d(t)$ is proportional to the single-atom emission spectrum and usually for the reliable Fourier transformation of $d(t)$, knowledge of $d(t)$ for a very large number of values of the argument t is necessary.

In the applications presented in this paper, we used for the function $F(t)$ [Eq. (B1)] the vector potential $\mathbf{A}(t)$ in the preferential gauge [20–22]

$$\mathbf{F}(t) = \mathbf{A}(t) = -\int_0^t \mathbf{E}(\tau) d\tau \ , \qquad (B8)$$

where $\mathbf{E}(t)$ is given by Eq. (3b)

$$\mathbf{E}(t) = f(t) \sum_{i=1}^{N_{\text{colors}}} \mathbf{E}_i \sin(\omega_i t + \varphi_i) \qquad (B9)$$

with temporal pulse shape $f(t)$ of the form of Eq. (10). The function $F(t)$ [Eqs. (B8) and (B9)] can be expanded in a Taylor series [Eq. (B6)] around any value of its argument t, where the derivatives $F^{(n)}(t_0)$ are simple analytic functions of $n, t_0, \omega_i, E_i, \varphi_i$ and of the parameters of Eq.

(10). The proof is omitted since it is straightforward but lengthy. It turned out that the present TSEM was, in most cases, about five times faster than the adaptive Bulirsch-Stöer [27] method for ordinary differential equations.

[1] K. C. Kulander, Phys. Rev. A **35**, 445 (1987).

[2] K. J. LaGattuta, Phys. Rev. A **41**, 5110 (1990); **47**, 1560 (1993).

[3] P. L. DeVries, J. Opt. Soc. Am. B **7**, 517 (1990).

[4] M. S. Pindzola, G. Bottrel, and C. Bottcher, J. Opt. Soc. Am. B **7**, 659 (1990).

[5] J. K. Liakos and M. Horbarsch, J. Opt. Soc. Am. B **7**, 685 (1990); J. Phys. B **24**, 3387 (1991).

[6] X. Tang, H. Rudolph, and P. Lambropoulos, Phys. Rev. Lett. **65**, 3269 (1990).

[7] M. S. Pindzola and M. Dörr, Phys. Rev. A **43**, 439 (1991).

[8] X. Tang and S. Basile, Phys. Rev. A **44**, R1454 (1991).

[9] K. C. Kulander, K. J. Schafer, and J. L. Krause, Phys. Rev. Lett. **66**, 2601 (1991).

[10] T.-F. Jiang and S.-I. Chu, Phys. Rev. A **46**, 7322 (1992).

[11] J. L. Krause, K. J. Schafer, and K. C. Kulander, Phys. Rev. A **45**, 4998 (1992).

[12] K. C. Kulander, K. J. Schafer, and J. L. Krause, in *Atoms in Intense Laser Fields,* edited by M. Gavrila (Academic, New York, 1992), p. 247.

[13] P. Lambropoulos and X. Tang, in *Atoms in Intense Laser Fields* (Ref. [12]), p. 335.

[14] S. Dionissopoulou, Th. Mercouris, A. Lyras, Y. Komninos, and C. A. Nicolaides (unpublished).

[15] C. A. Nicolaides and Th. Mercouris, Chem. Phys. Lett. **159**, 45 (1989).

[16] The use of field-free states as a basis assumes of course that the electronic structure and spectrum of the atom are not destroyed by the strength of the interaction. On the other hand, as we have already suggested [C. A. Nicolaides and Th. Mercouris, in *Atoms in Strong Fields,* edited by C. A. Nicolaides, C. W. Clark, and M. Nayfeh (Plenum, New York, 1990), p. 355], the use as a basis set of state-specific wave functions whose orbitals are field-dressed might be a topic for future research.

[17] C. A. Nicolaides, G. Aspromallis, and D. R. Beck, J. Mol. Struct. **199**, 283 (1989); Y. Komninos and C. A. Nicolaides, Phys. Rev. A **33**, 1995 (1986); Z. Phys. D **4**, 301 (1987); C. A. Nicolaides, in *Applied Many-Body Methods in Spectroscopy and Electronic Structure,* edited by D. Mukherjee (Plenum, New York, 1992), p. 233.

[18] We have also used the expansion approach of Eqs. (4) and (5) and $\mathcal{L}^2$ box-normalized vibrational continuum states for the computation of rates of molecular dissociation processes [Th. Mercouris, I. D. Petsalakis, and C. A. Nicolaides, Chem. Phys. Lett. **208**, 197 (1993); C. A. Nicolaides, Th. Mercouris, and I. D. Petsalakis, *ibid.* **212**, 685 (1993)]; Th. Mercouris, I. D. Petsalakis, P. Valtazauos and C. A. Nicolaides, J. Phys. B **27**, L519 (1994).

[19] K.-H. Yang, Ann. Phys. (N.Y.) **62**, 101 (1976).

[20] D. H. Kobe and A. Smirl, Am. J. Phys. **46**, 624 (1978); W. E. Lamb, Jr., R. R. Schlicker, and M. O. Scully, Phys. Rev. A **36**, 2763 (1987).

[21] F. H. M. Faisal, *Theory of Multiphoton Processes* (Plenum, New York, 1987).

[22] J. J. Forney, A. Quattropani, and F. Bassani, Nuovo Cimento **37**, 78 (1977); G. Grynberg and E. Giacobino, J. Phys. B **12**, L93 (1979); C. Leubner and P. Zoller *ibid.* **13**, 3613 (1980).

[23] J. L. Madajczyk and M. Trippenbach, J. Phys. A **22**, 2369 (1989); V. Veniard and B. Piraux, Phys. Rev. A **41**, 4019 (1990).

[24] P. L. Altick and E. N. Moore, Phys. Rev. **147**, 59 (1966).

[25] Since we work with the velocity form [Eq. (3a)], the expansion coefficients $a_i(n,t)$, $b_i(E,t)$ can be interpreted as probability amplitudes only for those time instants where the vector potential $A(t)$ vanishes [see Eq. (3d)]. $A(t)$ vanishes twice during an optical cycle of the field, thus giving the possibility of deducing rates or ATI spectra without performing the transformation of Eq. (3d), which is a time consuming and nontrivial task.

[26] N. Xu, Z. Phys. D **28**, 27 (1993); also see the papers in J. Opt. Soc. Am. B **7**, 403 (1990); and in *Atoms in Intense Laser Fields* (Ref. [12]).

[27] W. H. Press, B. P. Flannery, S. A. Teukolsky, and W. T. Vetterling, *Numerical Recipes* (Cambridge University Press, Cambridge, England, 1986), Chap. 15.

[28] S.-I. Chu and J. Cooper, Phys. Rev. A **32**, 2769 (1985).

[29] G. A. Kyrala and T. D. Nichols, Phys. Rev. A **44**, R1450 (1991).

[30] Th. Mercouris and C. A. Nicolaides, J. Phys. B **21**, L285 (1988).

[31] Th. Mercouris and C. A. Nicolaides, J. Phys. B **23**, 2037 (1990).

[32] The spectrum could be made more complicated by including higher thresholds and Li^- resonances. Although such a complex calculation is possible within the present scheme, it is postponed for the future since, for the intensities and photon energies used here, such higher-order contributions would not change the present conclusions.

[33] G. Peach, Mon. Not. R. Astron. Soc. **130**, 361 (1965).

[34] In Ref. [33] this term was set to zero as $R \rightarrow \infty$.

[35] A. Burgess, Proc. Phys. Soc. **81**, 442 (1963).

[36] J. A. Belling, J. Phys. B **1**, 136 (1968).

[37] In the applications presented in this paper, we chose ε to be 10^{-11}, which resulted in $N=20$. Also, the larger the time interval Δt, the larger the integer N. The value of Δt is of the order of one-tenth of the optical cycle.